Measurement and Modeling of a Complete Optical Absorption and Scattering by Coherent Surface Plasmon-Polariton Excitation Using a Silver Thin-Film Grating

Jae Woong Yoon,[1] Gang Min Koh,[2] Seok Ho Song,[2,*] and Robert Magnusson[1]
[1]*Department of Electrical Engineering, University of Texas-Arlington, Arlington, Texas 76019, USA*
[2]*Department of Physics, Hanyang University, Seoul 133-791, Korea*
(Received 31 January 2012; revised manuscript received 1 May 2012; published 21 December 2012)

We demonstrate the *plasmonic* analogue of a coherent photonic effect known as coherent perfect absorption. A periodically nanopatterned metal film perfectly absorbs multiple coherent light beams coupling to a single surface plasmon mode. The perfect absorbing state can be switched to a nearly perfect scattering state by tuning the phase difference between the incident beams. We theoretically explain the plasmonic coherent perfect absorption by considering time-reversal symmetry of surface plasmon amplification by stimulated emission of radiation. We experimentally demonstrate coherent control of the plasmonic absorption in good agreement with a coupled-mode theory of dissipative resonances. Associated potential applications include absorption-based plasmonic switches, modulators, and light-electricity transducers.

DOI: 10.1103/PhysRevLett.109.257402 PACS numbers: 78.66.Bz, 42.25.Hz, 73.20.Mf, 78.67.−n

The coherence properties of surface plasmons (SPs) are of immense scientific interest. Current research aims to strengthen fundamental understanding of SP coherence and enable potential applications to active nanoscale plasmonic devices [1–5]. In spite of the collective nature of SPs involving a large number of free electrons under the influence of scattering by thermal phonons and surface defects as well as electron scattering, experimental and theoretical studies have shown robust coherence of SPs within their propagation length scales. For example, Zia and Brongersma experimentally showed surface plasmon-polariton (SPP) interference patterns fundamentally identical to those found in the classical Young's double-slit experiment [1], and Tame *et al.* developed a theory describing the preservation of quantum statistics of coherent photons in SP modes on realistic lossy metal surfaces [2]. Rooted in coherent plasmonics, various active control systems have been proposed using spatially modulated laser beams on periodically perforated metal films [3], ultrashort pulses in tapered metal structures [4], and excited-carrier absorption in a quantum-dot layer in a nanoplasmonic interferometer system [5]. The coherence of SPs is also of special interest in quantum information processing following the observations of single-SP excitation in an Ag nanowire [6] and quantum entanglement of photonic spin eigenstates preserved during the SP-mediated transmission through metallic nanohole arrays [7].

Coherent perfect absorption (CPA) of light was recently demonstrated and explained by applying the idea of time-reversal symmetry of electromagnetism to light absorbing processes [8]. The *photonic* CPA is obtained by coherent coupling of two or more radiation modes to a single quasi-bound mode and interpreted as a time-reversed counterpart of coherent laser emission [9]. Recent theoretical study has shown that the CPA can be achieved in an arbitrary operating regime including transient, chaotic, or modulated optical fields [10]. Associated potential applications include absorption-based optical switches, modulators, and light-to-electricity transducers [11]. Developing the *plasmonic* analogue of this coherent photonic effect is of interest and may impact concomitant device applications. For instance, Noh *et al.* [12] theoretically demonstrated plasmonic CPA of multipole optical fields in metal nano wires and particles potentially applicable to ultrasensitive nanoscale probing and background-free spectroscopy.

In this Letter, we report the first experimental demonstration of *plasmonic* coherent absorption. Interpreted as a time-reversed counterpart to SP amplification by stimulated emission of radiation (SPASER) [13], a nanopatterned metal film perfectly absorbs multiple coherent beams under SPP resonance. The absorption can be switched to nearly perfect scattering depending on the phase difference between the incident beams. The plasmonic CPA considered in this paper differs in major aspects from that theoretically suggested by Noh *et al.* [12]. We treat a propagating SPP mode excited by plane waves as opposed to a localized SP mode excited by 2- or 3-dimensional multipole radiations [12] that require rather complex, delicate preparation of laser light in real experiments. We present rigorous numerical simulations that show plasmonic CPA with $\sim \times 75$ local field enhancement above that achieved in photonic CPA in a Si Fabry-Perot cavity [11]. Importantly, we experimentally observe coherent plasmonic absorption and obtain good agreement with theoretical predictions.

We consider the system shown in Fig. 1(a) where two transverse-magnetic (TM) polarized light waves illuminate a patterned Ag surface with period Λ at the phase-matching condition $k_{q,x} = k_{\mathrm{SP}} - 2\pi q/\Lambda$, where $k_{q,x}$ is an in-plane wave vector of the incident light, k_{SP} is the

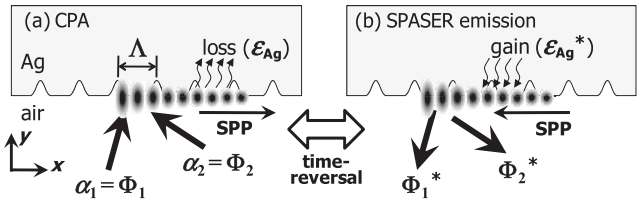

FIG. 1. (a) Schematic of plasmonic CPA with two coherent light waves with amplitudes α_1 and α_2 incident on a periodic Ag surface. The incoming waves couple to the SPP dissipating energy by Ohmic loss. Time reversing this situation corresponds to SPASER emission at threshold in (b) where the SPP is initially excited by gain from Ag with dielectric constant $\varepsilon_{Ag}{}^*$ and the SPP emits radiation $\beta_1 = \Phi_1{}^*$ and $\beta_2 = \Phi_2{}^*$.

propagation constant of the SPP, and an integer q represents a diffraction order. SPPs are coherently excited by each incident light wave for all available q's satisfying the radiation condition $|k_{q,x}| \leq \omega/c$, where ω is angular frequency and c is the speed of light in air.

We express a set of incoming waves with wave vector $k_{q,x}\mathbf{e}_x + k_{q,y}\mathbf{e}_y$ ($\mathbf{e}_j$ is the Cartesian unit vector) and amplitude α_q by a column vector $|\alpha\rangle$, and the corresponding set of outgoing waves with $k_{q,x}\mathbf{e}_x - k_{q,y}\mathbf{e}_y$ and β_q by $|\beta\rangle$, where the surface-normal wave vector component $k_{q,y} = [(\omega/c)^2 - k_{q,x}^2]^{1/2}$. The system response is described by a linear scattering matrix (S-matrix) equation as

$$|\beta\rangle = \boldsymbol{S}(\varepsilon_{Ag})|\alpha\rangle, \tag{1}$$

where ε_{Ag} is the complex dielectric constant of Ag. As explained in Refs. [8,11,14], CPA is obtained under two necessary conditions, the first requiring a vanishing S-matrix determinant

$$\det[\boldsymbol{S}(\varepsilon_{Ag})] = 0, \tag{2}$$

and the second requiring a coherent incoming wave configuration as

$$|\alpha\rangle = |\Phi\rangle, \tag{3}$$

where $|\Phi\rangle$ is given by the homogeneous simultaneous equations $\boldsymbol{S}(\varepsilon_{Ag})|\Phi\rangle = 0$.

The physics of these two conditions for CPA is explained theoretically by time-reversed SPASER emission at threshold [14], which can be treated as a linear scattering problem using the time-reversed form of Eq. (1)

$$|\alpha\rangle^* = \boldsymbol{S}(\varepsilon_{Ag}{}^*)|\beta\rangle^*. \tag{4}$$

As illustrated in Fig. 1(b), the SPASER emission in Eq. (4) is obtained by the time reversal of CPA in this system via loss-gain interchange, i.e., $\varepsilon_{Ag} \rightarrow \varepsilon_{Ag}{}^*$, and outgoing wave configuration $|\Phi\rangle^*$ in the absence of incoming waves, i.e., $|\alpha\rangle^* = |\Phi\rangle^*$ with $|\beta\rangle^* = 0$. The light-emission process from the SPASER in Fig. 1(b) operates with the gain-assisted initial excitation of a coherent, single-mode SPP followed by its leakage radiation $|\Phi\rangle^*$ as a coherent SPASER output. Thus, $|\Phi\rangle$ is interpreted as the conjugated leakage radiation from the SPP. In SPP amplification, the gain in the SPP exactly compensates radiation loss at threshold. The plasmonic CPA, as time-reversed lasing, thereby requires the internal (Ohmic) loss of the SPP to be identical to the radiation loss of the SPP. We can conclude that the vanishing determinant of $\boldsymbol{S}(\varepsilon_{Ag})$ in Eq. (2) is an equivalent representation of the critical coupling condition $\gamma_{nr} = \gamma_{rad}$, where γ_{nr} and γ_{rad} represent the SPP's nonradiative (internal) and radiative decay rates [14].

We numerically simulate plasmonic CPA arising on a periodic metal surface ($\Lambda = 700$ nm) possessing grooves with 25 nm depth and 175 nm half-width. A coordinate transformation algorithm known as the Chandezon method [15] is used for simulation. Silver is modeled as a Drude metal with plasma frequency of $\omega_p = 7.88$ eV and collision frequency of $\Gamma = f_{nr} \times 0.155$ eV [16] where Ohmic damping factor f_{nr} numerically adjusts absorption in Ag due to free-electron relaxation. The numerical value of f_{nr} is gradually tuned from 0 to 1 to obtain the critical coupling condition, i.e., $\gamma_{nr} = \gamma_{rad}$ or $\det[\boldsymbol{S}] = 0$. Note that tuning f_{nr} practically corresponds to temperature control as free-electron relaxation is mainly a result of random electron scattering by thermal phonons [17]. The collision frequency Γ can also be effectively tuned by surface absorbates that lead to an extra absorption due to the anomalous skin effect [18].

Figures 2(a) and 2(b) show angular spectra of the absorbance at $\lambda = 440$ and 580 nm, respectively. The absorption peaks marked by q have lateral spacing $(k_{q,x} - k_{q+1,x})/k_0 = \lambda/\Lambda$ as diffraction-coupled SPP resonances, where $k_0 = 2\pi/\lambda$. We estimate the total decay rates γ_{tot} of the SPP modes by measuring the absorption linewidth. Figure 2(c) and 2(d) shows a linear dependence of γ_{tot} on f_{nr}. The decay rates are obtained by $\gamma_{rad} = \gamma_{tot}(f_{nr} = 0)$ (solid square symbols) and $\gamma_{nr}(f_{nr}) = \gamma_{tot}(f_{nr}) - \gamma_{rad}$ [17]. Note that γ_{rad} can be taken to be independent of f_{nr} for $|\mathrm{Im}(\varepsilon_{Ag})| \ll |\mathrm{Re}(\varepsilon_{Ag})|$. With this approach, the critical coupling condition ($\gamma_{rad} = \gamma_{nr}$) is found at $f_{nr} = 0.4396$ for $\lambda = 440$ nm and 0.4837 for $\lambda = 580$ nm, respectively. At these two values of f_{nr} for the critical coupling condition, we numerically confirm that the CPA condition of Eq. (2) ($\det[\boldsymbol{S}] = 0$) is also satisfied as shown in Figs. 2(e) and 2(f).

CPA operation with two incident Gaussian beams is numerically demonstrated in Fig. 3 for $\lambda = 580$ nm at the critical coupling condition for $f_{nr} = 0.4837$. Figures 3(a) and 3(b) show that a single incoming beam at $q = 1$ or 2 couples to two outgoing beams. The surface-normal electric field (E_y) distribution in the inset of each panel shows a typical plasmonic behavior with the field decaying exponentially along the surface-normal direction. Coherent excitation by two beams is shown in Figs. 3(c) and 3(d).

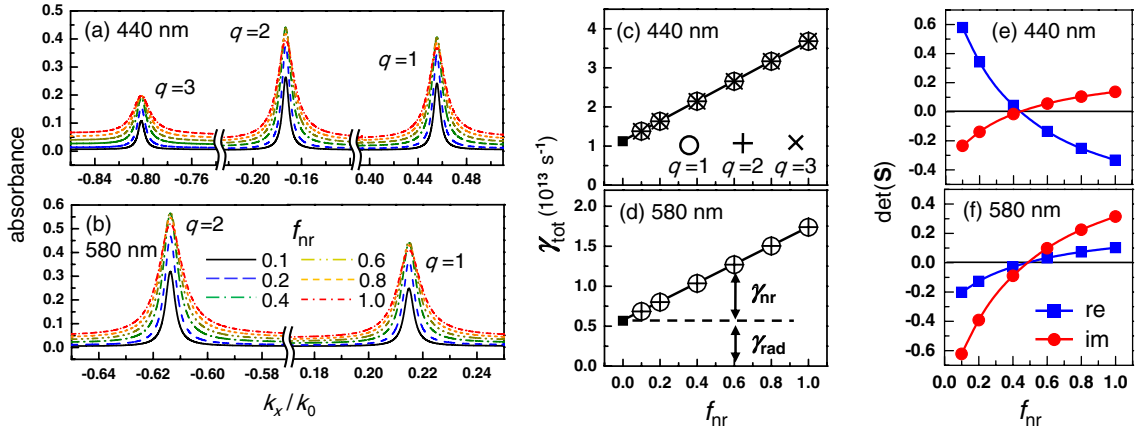

FIG. 2 (color online). Calculated angular spectrum of the absorbance relative to Ohmic damping factor f_{nr} at (a) $\lambda = 440$ nm and (b) $\lambda = 580$ nm; (c) and (d) show total decay rate γ_{tot} of the SPP obtained by measuring absorbance linewidth. γ_{rad} is estimated by linearly extrapolating γ_{tot} (solid square symbols) to $f_{nr} = 0$ as schematically indicated in (d). Panels (e) and (f) show the dependence of det($\boldsymbol{S}$) on f_{nr} at $\lambda = 440$ nm and 580 nm. Real (blue squares) and imaginary (red circles) parts of det($\boldsymbol{S}$) simultaneously vanish at $f_{nr} = 0.44$ for $\lambda = 440$ nm in (e) and at $f_{nr} = 0.48$ for $\lambda = 580$ nm in (f).

In-phase excitation when $|\alpha\rangle = |\Phi\rangle$ in Fig. 3(c) clearly demonstrates CPA with no outgoing beams and maximally enhanced surface field due to the SPP. Outgoing power in this case is 6×10^{-8} of the incoming power and $|\boldsymbol{E}|^2$ at the interface is $\sim \times 150$ stronger than the incoming field. Note that $|\boldsymbol{E}|^2$ enhancement factor for the CPA demonstrated in Ref. [11] is estimated to $\sim \times 2$ based on the measured Fabry-Perot resonance linewidth and optical cavity length therein. On the contrary, for out-of-phase excitation in Fig. 3(d) where the incoming beam at $q = 2$ has π-phase difference from the in-phase case, almost all of the incoming power (96%) is transferred to the outgoing beams with negligible field enhancement at the interface. This demonstrates a phase-controlled transition between perfect absorption and nearly total scattering. See the Supplemental movie [19] (online) for the continuous transition by incident phase control.

Corresponding to the numerical simulation in Figs. 3(a) and 3(b), we experimentally realize plasmonic coherent absorption on a surface-relief Ag grating with 723.7 nm period and 63.1 nm depth on a silicon substrate as shown in Figs. 4(a) and 4(b). Optical response of the fabricated device with a single incident beam at wavelength 632.8 nm is shown in Fig. 4(c). The measured diffraction efficiencies and absorbance show SPP resonances at incident angles $\theta_1 = 9.2°$ ($q = 1$) and $\theta_2 = -45.7°$ ($q = 2$) with peak SPP absorbance measured as $A(\theta_1) = A_1 = 0.493$ and $A(\theta_2) = A_2 = 0.402$. At both SPP resonance angles, the incident beam couples to two reflection orders (R_0 and R_{-1}) as modeled numerically in Figs. 3(a) and 3(b).

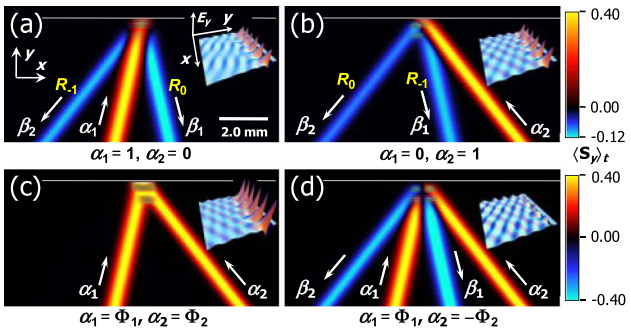

FIG. 3 (color online). CPA by two coherent Gaussian laser beams at $\lambda = 580$ nm. The white, horizontal line near the top of each panel indicates the Ag grating surface. Each panel shows the surface-normal component of the time-averaged Poynting vector. The 3D surface plot in the inset shows surface-normal electric field distribution in the optical near field at the incident beam center. (a) Single beam excitation at $q = 1$. (b) Single beam excitation at $q = 2$. (c) Coherent in-phase excitation for $(\alpha_1, \alpha_2) = (\Phi_1, \Phi_2)$. (d) Coherent out-of-phase excitation for $(\alpha_1, \alpha_2) = (\Phi_1, -\Phi_2)$.

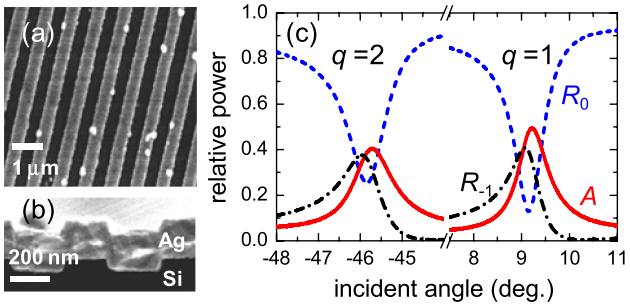

FIG. 4 (color online). Scanning electron micrograph of the fabricated Ag grating on Si substrate: (a) top view and (b) the cross section. (c) Measured angular spectra of the diffraction efficiencies (R_0 and R_{-1}) and the absorbance (A) near SPP resonance conditions at $\theta = 9.215°$ ($q = 1$) and $-45.712°$ ($q = 2$). He-Ne laser ($\lambda = 632.8$ nm) was used for the measurement.

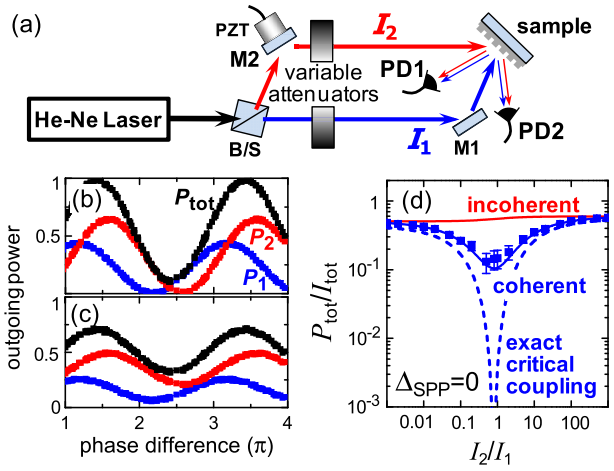

FIG. 5 (color online). (a) Schematic of the Mach-Zehnder type interferometer used for phase-controlled absorption measurements. Two laser beams at $q = 1$ (I_1, blue) and 2 (I_2, red) are incident on the sample. Piezoelectric mirror ($M2$) controls phase difference between I_1 and I_2. PD1 and PD2 (Si photodiodes) measure outgoing power P_1 at $q = 1$ and P_2 at $q = 2$, respectively. Measured P_1 (blue), P_2 (red), and their total $P_{tot} = P_1 + P_2$ (black) are presented in (b) for incident power ratio $I_2/I_1 = A_2/A_1 = 0.815$ and in (c) for $I_2/I_1 = 0.05$. (d) Coherent (blue) and incoherent (red) outgoing optical power with varying incident power ratio I_2/I_1. Symbols with vertical error bars correspond to experiment and the curves represent theory.

Coherent response of the plasmonic absorption with two-beam excitation is observed by using a Mach-Zehnder interferometer. Figure 5(a) shows a schematic of the measurement system. A piezoelectric mirror ($M2$) in the beam path at $q = 2$ (red arrows) controls the phase difference, and two variable attenuators are inserted in the two beam paths to independently change the incoming power $I_q = |\alpha_q|^2$. A linearly polarized (500:1) He-Ne laser at 632.8 nm is used as a coherent light source. This laser with linewidth 2 pm and coherence length around 20 cm is practically acceptable as a pure monochromatic coherent source when compared to the plasmonic absorption bandwidth of ~18 nm.

We measure outgoing powers of the two reflected beams, $P_1 = |\beta_1|^2$ at θ_1 and $P_2 = |\beta_2|^2$ at θ_2. Figure 5(b) shows the phase-sensitive behavior of P_1, P_2, and $P_{tot} = P_1 + P_2$ when the coherent absorption is maximized for $I_2/I_1 = 0.815$. For different incoming power ratios, coherent modulation of the absorption is smaller as shown in Fig. 5(c) for $I_2/I_1 = 0.05$.

The phase-controlled modulation of the outgoing power is described by an interference formula due to the coupled-mode model of a dissipative quasibound resonator [14] as

$$P_{tot} = I_{tot} - A_1 I_1 - A_2 I_2 - 2(A_1 A_2 I_1 I_2)^{1/2} \cos\Delta_{SPP}, \quad (5)$$

where $I_{tot} = I_1 + I_2$ is total incoming power and Δ_{SPP} is phase difference between two coherent SPPs excited by I_1 and I_2, respectively. Equation (5) describes P_{tot} in Figs. 5(b) and 5(c), respectively. The outgoing power can be minimized to

$$[P_{tot}]_{min} = (1 - A_1 - A_2) I_{tot}, \quad (6)$$

when the SPP is maximally excited for $\Delta_{SPP} = 0$ and the incoming powers satisfy $I_2/I_1 = A_2/A_1$. In Fig. 5(b), $I_2/I_1 = 0.815$ for maximal coherent absorption is well consistent with $A_1/A_2 = 0.814$ obtained from the measured absorbance in Fig. 4(c).

In Fig. 5(d), we present coherent (blue solid curve) and incoherent (red curve) dependences of P_{tot} at $\Delta_{SPP} = 0$ on the incoming power ratio I_2/I_1. P_{tot} for the incoherent case (red curve) is given by

$$[P_{tot}]_{incoherent} = I_{tot} - A_1 I_1 - A_2 I_2, \quad (7)$$

from Eq. (5) with $\cos\Delta_{SPP} = 0$ (random-phase averaged out). Good agreement of the experimental results with the theory shows validity of Eq. (6). The error in the measurement originates from phase fluctuation due to acoustic vibration.

At the critical coupling condition, i.e., $\gamma_{rad} = \gamma_{nr}$, $A_1 + A_2 = 1$ and $[P_{tot}]_{min} = 0$ as indicated by blue dotted curve in Fig. 5(d). We note that the experimental result differs from the ideal case for exact critical coupling condition; namely, the absorption is not perfect, as seen in Fig. 5(d) with $[P_{tot}]_{min} = 0.117$. Imperfect performance in the experiment is due to some mismatch between γ_{rad} and γ_{nr}; i.e., the critical coupling condition is not precisely achieved. Reducing geometrical errors in the grating fabrication will achieve improved results corresponding to the dashed curve in Fig. 5(d). We note that use of finite beams with nonzero divergence is another possible origin of the imperfect agreement. The laser beam used in the experiment can be approximated to a Gaussian beam with diameter ~2 mm and divergence 0.02°. When we compare these values with propagation length of the SPP mode of ~22 μm and angular bandwidth of the resonance ~1°, we find that the effect of finite beam size and divergence is negligible.

In summary, we have demonstrated plasmonic coherent perfect absorption of light incident on a nanopatterned metal film. Rigorous numerical simulation modeling two Gaussian laser beams incident on a metallic grating shows phase-sensitive switching between plasmonic CPA and nearly total scattering. This phase-controlled absorbing device is experimentally demonstrated to operate in good agreement with an analytical description based on the coupled-mode theory of a dissipative quasibound resonator [14]. In addition to strong field enhancement and subwavelength localization properties, the plasmonic CPA has two advantages in practical instrumentation. First, the critical coupling condition can be achieved at arbitrary wavelengths by designing appropriate surface geometry. Second, the outgoing beam paths can be freely selected by choice of the period of the surface patterning. Further development of the plasmonic CPA in metallic nanoslit

arrays [20] and tapered nanofocusing systems [21] may realize phase-controlled, active plasmonics elements providing extremely strong light localization and nonlinear interactions at deep subwavelength scales.

This work was supported by the Industrial Strategic Technology Development Program (KI001804) of the MKE, Korea. Additional support was provided by the Texas Instruments Distinguished University Chair in Nanoelectronics endowment.

Note added in proof.—After we submitted this Letter, during the peer-review phase, we became aware of similar work reporting plasmonic coherent absorption and transmission in a thin film of metallic metamaterial [22].

*Corresponding author.
shsong@hanyang.ac.kr

[1] R. Zia and M. L. Brongersma, Nat. Nanotechnol. **2**, 426 (2007).
[2] M. S. Tame, C. Lee, J. Lee, D. Ballester, M. Paternostro, A. V. Zayats, and M. S. Kim, Phys. Rev. Lett. **101**, 190504 (2008).
[3] B. Gjonaj, J. Aulbach, P. M. Johnson, A. P. Mosk, L. Kuipers, and A. Lagendijk, Nat. Photonics **5**, 360 (2011).
[4] M. Durach, A. Rusina, and M. I. Stockman, Nano Lett. **7**, 3145 (2007).
[5] D. Pacifici, H. J. Lezec, and H. A. Atwater, Nat. Photonics **1**, 402 (2007).
[6] A. V. Akimov, A. Mukherjee, C. L. Yu, D. E. Chang, A. S. Zibrov, P. R. Hemmer, H. Park, and M. D. Lukin, Nature (London) **450**, 402 (2007).
[7] E. Altewischer, M. P. van Exter, and J. P. Woerdman, Nature (London) **418**, 304 (2002).
[8] Y. D. Chong, L. Ge, H. Cao, and A. D. Stone, Phys. Rev. Lett. **105**, 053901 (2010).
[9] H. Cao, Y. G. Zhao, S. T. Ho, E. W. Seelig, Q. H. Wang, and R. P. H. Chang, Phys. Rev. Lett. **82**, 2278 (1999).
[10] S. Longhi and G. D. Valle, Phys. Rev. A **85**, 053838 (2012).
[11] W. Wan, Y. Chong, L. Ge, H. Noh, A. D. Stone, and H. Cao, Science **331**, 889 (2011).
[12] H. Noh, Y. Chong, A. Douglas Stone, and H. Cao, Phys. Rev. Lett. **108**, 186805 (2012).
[13] D. J. Bergman and M. I. Stockman, Phys. Rev. Lett. **90**, 027402 (2003).
[14] J. Yoon, K. H. Seol, S. H. Song, and R. Magnusson, Opt. Express **18**, 25702 (2010).
[15] J. Chandezon, M. T. Dupuis, G. Cornet, and D. Maystre, J. Opt. Soc. Am. **72**, 839 (1982).
[16] E. D. Palik, *Handbook of Optical Constants of Solids II* (Academic Press, San Diego, 1988).
[17] J. Yoon, S. H. Song, and J.-H. Kim, Opt. Express **16**, 1269 (2008).
[18] B. N. J. Persson, Phys. Rev. B **44**, 3277 (1991).
[19] See Supplemental Material at http://link.aps.org/supplemental/10.1103/PhysRevLett.109.257402 for the animation showing the continuous transition between the CPA and nearly total scattering states.
[20] F. J. Carcia-Vidal, L. Martin-Moreno, T. W. Ebbesen, and L. Kuipers, Rev. Mod. Phys. **82**, 729 (2010).
[21] M. I. Stockman, Phys. Rev. Lett. **93**, 137404 (2004).
[22] J. Zhang, K. F. MacDonald, and N. I. Zheludev, Light: Science and Applications **1**, e18 (2012).